

## Formation of a Ruthenium(V)—Imido Complex and the Reactivity in Substrate Oxidation in Water through the Nitrogen Non-Rebound Mechanism

Tomoya Ishizuka,<sup>†</sup> Taichi Kogawa,<sup>†</sup> Misaki Makino,<sup>†</sup> Yoshihito Shiota,<sup>‡</sup> Kazuaki Ohara,<sup>§</sup> Hiroaki Kotani,<sup>†</sup> Shunsuke Nozawa,<sup>||</sup> Shin-ichi Adachi,<sup>||</sup> Kentaro Yamaguchi,<sup>§</sup> Kazunari Yoshizawa,<sup>‡</sup> and Takahiko Kojima<sup>\*,†</sup>

<sup>†</sup>Department of Chemistry, University of Tsukuba, 1-1-1 Tennoudai, Tsukuba, Ibaraki 305-8571, Japan

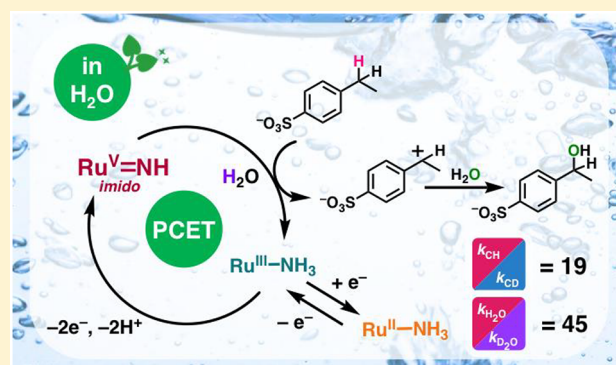
<sup>‡</sup>Institute for Materials Chemistry and Engineering, Kyushu University, Motooka, Nishi-Ku, Fukuoka 819-0395, Japan

<sup>§</sup>Faculty of Pharmaceutical Sciences at Kagawa Campus, Tokushima Bunri University, 1314-1 Shido, Sanuki, Kagawa 769-2193, Japan

<sup>||</sup>Photon Factory, Institute of Materials Structure Science, High Energy Accelerator Research Organization (KEK), 1-1 Oho, Tsukuba, Ibaraki 305-0801, Japan

### Supporting Information

**ABSTRACT:** A Ru<sup>II</sup>—NH<sub>3</sub> complex, **2**, was oxidized through a proton-coupled electron transfer (PCET) mechanism with a Ce<sup>IV</sup> complex in water at pH 2.5 to generate a Ru<sup>V</sup>=NH complex, **5**. Complex **5** was characterized with various spectroscopies, and the spin state was determined by the Evans method to be *S* = 1/2. The reactivity of **5** in substrate C—H oxidation was scrutinized in acidic water, using water-soluble organic substrates such as sodium ethylbenzene-sulfonate (EBS), which gave the corresponding 1-phenylethanol derivative as the product. In the substrate oxidation, complex **5** was converted to the corresponding Ru<sup>III</sup>—NH<sub>3</sub> complex, **3**. The formation of 1-phenylethanol derivative from EBS and that of **3** indicate that complex **5** as the oxidant does not perform nitrogen-atom transfer, in sharp contrast to other high-valent metal—imido complexes reported so far. Oxidation of cyclobutanol by **5** afforded only cyclobutanone as the product, indicating that the substrate oxidation by **5** proceeds through a hydride-transfer mechanism. In the kinetic analysis on the C—H oxidation, we observed kinetic isotope effects (KIEs) on the C—H oxidation with use of deuterated substrates and remarkably large solvent KIE (sKIE) in D<sub>2</sub>O. These positive KIEs indicate that the rate-determining step involves not only cleavage of the C—H bond of the substrate but also proton transfer from water molecules to **5**. The unique hydride-transfer mechanism in the substrate oxidation by **5** is probably derived from the fact that the Ru<sup>IV</sup>—NH<sub>2</sub> complex (**4**) formed from **5** by 1e<sup>−</sup>/1H<sup>+</sup> reduction is unstable and quickly disproportionates into **3** and **5**.



## INTRODUCTION

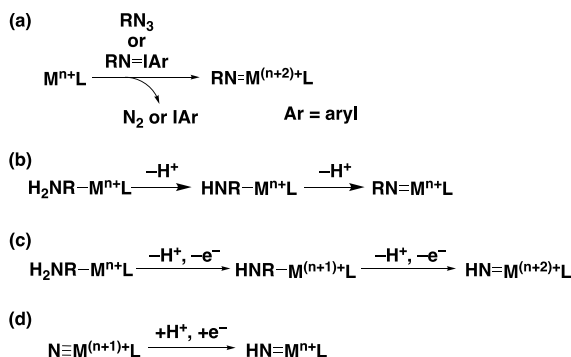
The development of the selective oxidation of C—H bonds in organic substrates is of great importance in modern chemistry. High-valent metal—oxo complexes have been intensively investigated as responsible species in the C—H bond oxidation as observed for cytochrome P-450 and methane monooxygenase.<sup>1</sup> A number of synthetic metal—oxo complexes have been prepared and have served as functional models of the reactive intermediates to elucidate the reaction mechanisms and to develop efficient and selective oxidation reactions.<sup>2</sup> As analogues of high-valent metal—oxo complexes, high-valent metal—nitrido (M≡N) complexes have been recognized as a quite important class of compounds,<sup>3–7</sup> since they have been known as active species in nitrogen-atom-transfer reactions

such as aziridination and C—H amination.<sup>3,8,9</sup> High-valent metal—imido (M=NR; R = alkyl or aryl) complexes have been also well investigated as useful reagents for nitrogen insertion to organic substances.<sup>10–13</sup> Imido ligands are dianionic, and thus, the impact on the stabilization of high-valent metal species is weaker than trianionic nitride ligands;<sup>14</sup> however, due to the lower stability, the reactivity of M=NR complexes is expected to be higher than that of high-valent M≡N complexes, when the valence numbers of the metal centers are the same.<sup>10</sup> The most typical procedure to form metal—imido species is a reaction of a metal complex with an

Received: June 15, 2019

alkyl or aromatic azide (RN<sub>3</sub>) through dinitrogen elimination<sup>15,16</sup> or with an iminophenyliodinane derivative (RN=IAr) through nitrogen atom transfer (Scheme 1a).<sup>17</sup>

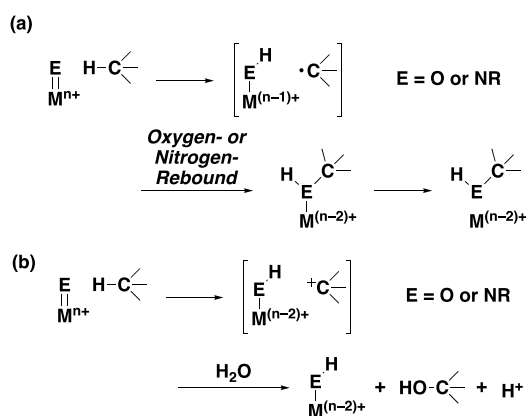
Scheme 1. Formation of Metal–Imido Complexes



Protonation of metal–nitrido complexes or deprotonation of metal–amine complexes (M–NH<sub>2</sub>R) have been also applied to obtain metal–imido complexes (Scheme 1b).<sup>18,19</sup> Another possible procedure to obtain high-valent metal–imido complexes is proton-coupled electron-transfer (PCET) oxidation of metal–amine (M–NH<sub>3</sub>) or M–NH<sub>2</sub>R complexes (Scheme 1c)<sup>20,21</sup> or PCET reduction of the corresponding metal–nitrido complex (Scheme 1d).<sup>22</sup> Using the PCET procedures, complexes in various valence states can be readily obtained in the case where the stability of oxidized species is assured. Based on the stability, detailed mechanistic insights into the oxidation reactions can be gained with the obtained high-valent species. Moreover, the PCET procedures produce no chemical waste such as iodobenzene, which is formed with the imino–iodinane method to form an imido complex,<sup>17</sup> and thus, the procedure is atom-economical. However, the previous trials to synthesize high-valent metal–nitrido or –imido complexes using PCET methods in water resulted in the formation of the corresponding metal–nitrosyl complex,<sup>23,24</sup> probably because the formed high-valent species reacted with a water molecule used as the solvent. Therefore, the high-valent metal–nitrido and –imido complexes formed through PCET procedures have never been well characterized experimentally and have been just proposed as undetected intermediates.<sup>23,24</sup>

On the other hand, in the C–H oxidation reactions with high-valent metal–oxo complexes as the active species,<sup>3,25–29</sup> the H-atom abstraction has been generally considered to occur as the first step, affording the one-electron-reduced metal–hydroxo species and a nascent carbon radical. The hydroxyligand is rebound to the carbon radical to give the product (Scheme 2a).<sup>29</sup> Metal–nitrido and –imido complexes have been also reported to perform H-atom abstraction from a C–H bond of organic substrates and afford aminated products through a nitrogen-rebound process.<sup>9,30</sup> Therefore, to reform a M–NH<sub>3</sub> complex for persisting the metal–nitrido or –imido complexes into PCET catalytic systems, the vacant coordination site formed by the nitrogen rebound needs to be refilled with ammonia or an appropriate amine. An alternative mechanism in the C–H oxidation is hydride transfer in water to afford a hydroxylated product (Scheme 2b).<sup>29</sup> However, examples of substrate oxidation by metal–oxo complexes proceeding through a hydride-transfer mechanism are very rare,<sup>31</sup> and as far as we know, no report has been

Scheme 2. Hydrogen-Atom Transfer (a) and Hydride Transfer (b) to High-Valent Metal Complexes



provided on such a hydride-transfer mechanism by metal–nitrido and –imido complexes.

Herein, we report the formation and spectroscopic characterization of an unprecedented Ru<sup>V</sup>=NH complex through PCET oxidation of the corresponding Ru<sup>II</sup>–amine complex. The reactivity of the Ru<sup>V</sup>=NH complex in C–H oxidation in water has been thoroughly investigated on the basis of kinetic analysis. In stark contrast to the cases of high-valent metal–nitrido or –imido complexes reported so far, the imido nitrogen atom of the Ru<sup>V</sup>=NH complex remained at the Ru center after the C–H oxidation to recover the ammine ligand without going through the nitrogen-rebound mechanism.<sup>9</sup> The C–H oxidation by the Ru<sup>V</sup>=NH complex in water has been revealed to proceed through a hydride-transfer mechanism accompanied by proton transfer from a water molecule.

## RESULTS AND DISCUSSION

**Synthesis of the Ru<sup>II</sup>–NH<sub>3</sub> Complex 2.** In this study, we utilized *N,N*-bis(2-pyridylmethyl)-*N*-bis(2-pyridyl)-methylamine (N4Py)<sup>32</sup> as a pentadentate ancillary ligand. The advantages of the N4Py ligand are as follows: (1) the ligand acts a pentadentate ligand to occupy the five coordination sites of an octahedral Ru center leaving one ammine- or imido-ligation site; (2) no isomerization can be expected; and (3) the metal center can be relatively electron-rich due to the strong  $\sigma$ -donation from the tertiary amino nitrogen (N1 in Figure 1), located at the *trans*-position of the

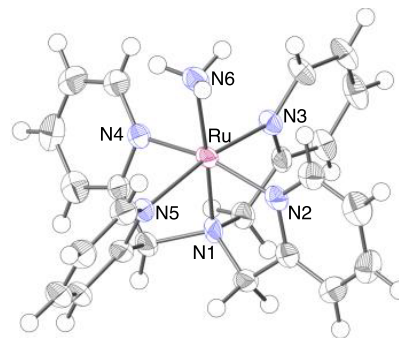
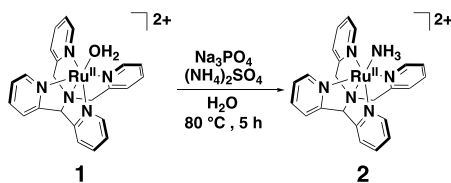


Figure 1. Crystal structure of the cationic part of 2. PF<sub>6</sub><sup>−</sup> ions are omitted for clarity. The thermal ellipsoids are drawn with 50% probability level.

imido ligand to be formed. The Ru<sup>II</sup>–ammine complex, **2**, was synthesized from [Ru<sup>II</sup>(N<sub>4</sub>Py)(OH<sub>2</sub>)](PF<sub>6</sub>)<sub>2</sub> (**1**)<sup>28c</sup> as a starting material, which was treated with (NH<sub>4</sub>)<sub>2</sub>SO<sub>4</sub> and Na<sub>3</sub>PO<sub>4</sub> in water (Scheme 3).<sup>24</sup> The characterization of **2** was

### Scheme 3. Synthesis of a Ru<sup>II</sup>–NH<sub>3</sub> Complex, **2**



conducted with <sup>1</sup>H NMR spectroscopy (Figures S1–S3), and ESI-TOF-MS spectrometry (Figure S4). The crystal structure of **2** was explicitly revealed by single-crystal X-ray crystallography (Figure 1). One of the structural characteristics of **2** is found in the bond distance between the Ru<sup>II</sup> center and the N1 atom, i.e., 1.967(5) Å for the corresponding aqua complex **1**<sup>28c</sup> and 2.039(3) Å for **2**. This elongation of the Ru–N1 bond distance in **2** relative to that of **1** is probably caused by the strong *trans*-influence of the ammine ligand compared to that of the aqua ligand.<sup>33</sup> In addition, the Ru–N6 bond length is 2.167(4) Å, which is also elongated relative to those bonds in Ru<sup>II</sup>–NH<sub>3</sub> complexes reported in literature (2.08–2.12 Å).<sup>24a,34</sup> by the *trans* influence of the strongly  $\sigma$ -donating tertiary amino nitrogen.

**Characteristics of **2** and Its Redox Properties.** The pH dependency of the UV–vis spectra of **2** in an aqueous solution was examined in the pH range of 1.5–12 (Figure S5). However, no spectral change was observed in the pH range, indicating that the ammine ligand of **2** does not undergo deprotonation in this pH range. Additionally, in the <sup>1</sup>H NMR spectrum of **2** in D<sub>2</sub>O (pD 7.4),<sup>35</sup> the <sup>1</sup>H NMR signal of the ammine ligand was clearly observed at 3.21 ppm with the integral ratio of 3H (Figure S1). Worthy of note, the NH<sub>3</sub> signal did not disappear through H–D exchange with the solvent, even after dissolving in D<sub>2</sub>O for 24 h. Therefore, the ammine ligand is intact without deuterium exchange or deprotonation in the pH range of 1.5–12.<sup>36</sup> On the other hand, upon labeling with the <sup>15</sup>N nucleus of the ammine nitrogen, the <sup>1</sup>H NMR signal of the ammine N–H protons at  $\delta$  3.21 split into a doublet ( $J_{\text{NH}} = 68$  Hz) due to the coupling with the <sup>15</sup>N nuclear spin ( $I = 1/2$ ) (Figure S6). Therefore, the <sup>1</sup>H NMR signal at  $\delta$  3.21 is clearly assigned to N–H of the ammine ligand.

Based on the deprotonation inertness of **2** and the electrochemical studies of **2** at various pHs (Figure S7), we provided the Pourbaix diagram of **2** as depicted in Figure 2. In the lower pH region, three oxidation peaks were observed in the differential-pulse voltammograms (DPVs) (Figure S7a). The Ru<sup>II</sup>/Ru<sup>III</sup> redox potential was independent of the pH change, and slopes for the Ru<sup>III</sup>/Ru<sup>IV</sup> and Ru<sup>IV</sup>/Ru<sup>V</sup> processes were –60 and –53 mV/pH, respectively. This result clearly indicates that both processes consist of 1e<sup>–</sup>/1H<sup>+</sup> PCET and complex **2** can form a high-valent Ru<sup>V</sup>–imido (Ru<sup>V</sup>=NH) complex by PCET oxidation in the pH region. In the basic region, the first redox wave showed the doubled current relative to that of the second wave (Figure S7c). The slopes of the first and second processes are –55 and –59 mV/pH, respectively, and thus, the processes are ascribable to 2e<sup>–</sup>/2H<sup>+</sup> and 1e<sup>–</sup>/1H<sup>+</sup> PCET, respectively, in the basic region. It is

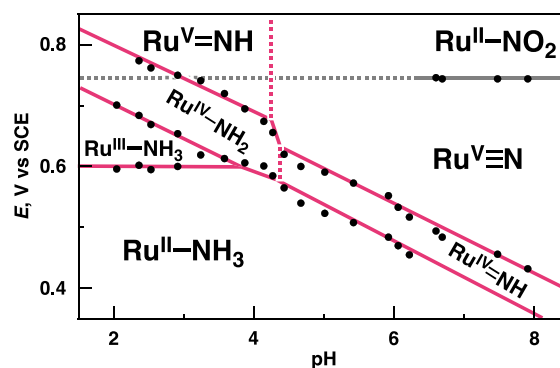
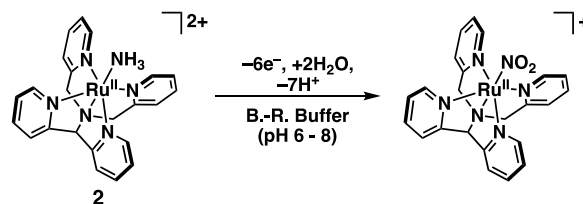


**Figure 2.** Pourbaix diagram of **2**. The redox potential at each pH was obtained from the DPV of **2** in Britton–Robinson buffer (see Figure S7), whose pH was adjusted with addition of NaOH aq.

noteworthy that in the pH range of 6–8, an oxidation wave was observed at +0.74 V vs SCE and was intact regardless of the pH change. We assigned this process as the formation of a Ru<sup>II</sup>–nitro complex formed in the course of PCET oxidation of **2** in water (Scheme 4). Actually, we could obtain

### Scheme 4. Formation of a Ru<sup>II</sup>–Nitro Complex from **2** in pH 6–8



[Ru<sup>II</sup>(NO<sub>2</sub>)(N<sub>4</sub>Py)]<sup>+</sup> as the product using 10 equiv of (NH<sub>4</sub>)<sub>2</sub>[Ce<sup>IV</sup>(NO<sub>3</sub>)<sub>6</sub>] (CAN) as an electron-transfer oxidant at pD 7.4. This process has been reported as a reaction with a water molecule to form the nitro ligand through the formation of a putative high-valent Ru=NH complex.<sup>23</sup>

**Chemical Oxidation of **2**.** Based on the Pourbaix diagram in Figure 2, we performed PCET oxidation of **2** with CAN as an oxidant. The reaction was monitored with the <sup>1</sup>H NMR spectroscopy (Figure 3 and Figure S9). Upon addition of 1 equiv of CAN to the D<sub>2</sub>O solution of **2** (pD 2.9<sup>35</sup>) at 277 K, the diamagnetic <sup>1</sup>H NMR signals of **2** disappeared completely and even paramagnetic signals were not observed in the range of –70–+80 ppm (Figure 3b). Further addition of 1 equiv of CAN allowed us to observe paramagnetically shifted signals in the range of –40–+30 ppm (Figure 3c), and the peak intensities of the paramagnetically shifted signals relative to that of the internal reference (DSS) were doubled by adding one more equiv of CAN (Figure 3d). Therefore, addition of 1 equiv of CAN to the solution of **2** gives the corresponding Ru<sup>III</sup>–NH<sub>3</sub> complex (**3**), and further oxidation with one more equivalent of CAN tentatively affords the corresponding Ru<sup>IV</sup>–NH<sub>2</sub> complex (**4**), which quickly disproportionates into **3** and the Ru<sup>V</sup>=NH complex (**5**) (Scheme 5). This disproportionation is rationalized in light of the narrow potential gap between the Ru<sup>III</sup>/Ru<sup>IV</sup> and Ru<sup>IV</sup>/Ru<sup>V</sup> couples in the Pourbaix diagram (Figure 2).<sup>37</sup> To confirm the formation of the Ru<sup>III</sup> species, **3**, we measured an ESR spectrum of an aqueous solution of **2** after addition of 1 equiv of CAN. In the ESR spectrum (Figure S8), a rhombic signal

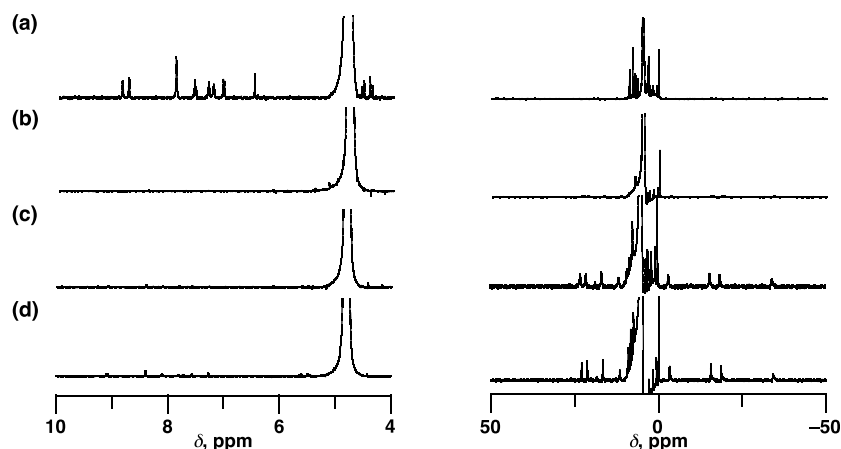
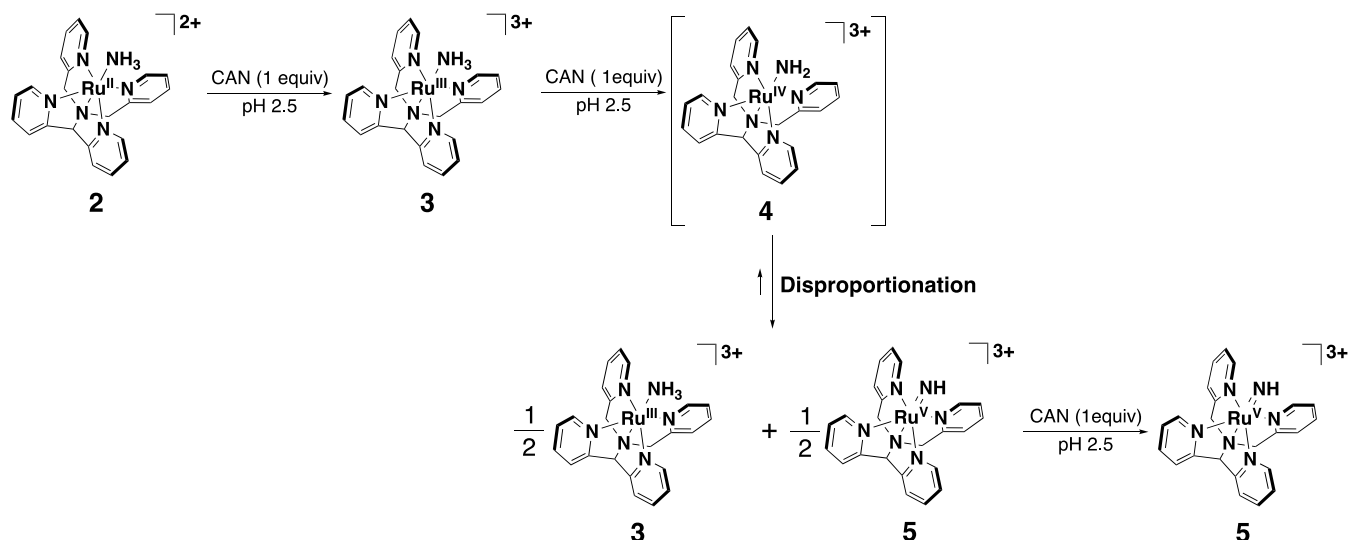


**Figure 3.**  $^1\text{H}$  NMR spectral change upon the oxidation of **2** with CAN as an oxidant in  $\text{D}_2\text{O}$  (pD 2.9), including DSS as an internal standard, at 277 K: (a) **2**, (b) **2** + 1 equiv of CAN, (c) **2** + 2 equiv of CAN, and (d) **2** + 3 equiv of CAN (left: the diamagnetic region; right: expanded region).

**Scheme 5.** PCET Oxidation of **2** to Afford the Corresponding  $\text{Ru}^{\text{V}}=\text{NH}$  Complex, **5**



was observed at  $g_1 = 2.584$ ,  $g_2 = 2.158$ ,  $g_3 = 1.857$ , and  $g_{\text{av}} = 2.200$ , which are in the typical range for  $\text{Ru}^{\text{III}}$  complexes ( $S = 1/2$ ).<sup>38</sup> Addition of two more equivalents of CAN (3 equiv in total) produced the quantitative amount of **5**. When this reaction was done not at 277 K but at room temperature, the formation of a  $\text{Ru}^{\text{II}}$ -nitrosyl complex,  $[\text{Ru}^{\text{II}}(\text{N}_4\text{Py})(\text{NO})]^{3+}$  (**6**), was observed (Figure S10).<sup>39</sup>

To confirm the reversibility of the redox processes of **2** to form **5**, a  $2e^-$ -reductant, 1,4-hydroquinone ( $\text{H}_2\text{Q}$ ), was added as a reductant to the solution of **5** at 277 K, and  $^1\text{H}$  NMR spectral changes were observed (Figure S11). Upon addition of 0.5 mol equiv of  $\text{H}_2\text{Q}$ , the paramagnetic  $^1\text{H}$  NMR signals of **5** decreased to half the intensity, which indicates the disproportionation of **4**, and further addition of 0.5 mol equiv of  $\text{H}_2\text{Q}$  caused disappearance of the any  $^1\text{H}$  NMR signals due to the formation of **3**. Addition of further 0.5 mol equiv of  $\text{H}_2\text{Q}$  afforded the distinctive  $^1\text{H}$  NMR signals of **2**, and the recovery yield was quantitative on the basis of peak integration. Note that no signals derived from **6** were observed in the  $^1\text{H}$  NMR spectra in the course of the reduction with  $\text{H}_2\text{Q}$ . Therefore, we conclude that the redox behavior of **2** to give the  $\text{Ru}^{\text{V}}$  complex **5** is quite reversible at 277 K.

**Characterization of 5.** Characterization of **5** was performed with high-resolution (HR) ESI-TOF-MS spectrometry,  $^1\text{H}$  NMR and IR spectroscopies, XANES measurements, and DFT calculations. The HR-ESI-TOF-MS spectrum of **5**, which was prepared by treatment of **2** with 3 equiv of CAN in acidic water (pH 2.5) and diluted with  $\text{CH}_3\text{CN}$  to set the solvent ratio as  $\text{CH}_3\text{CN}/\text{H}_2\text{O} = 1:2$ , exhibits a peak cluster at 161.365, which matches the simulated value for  $[\text{Ru}(\text{NH})(\text{N}_4\text{Py})]^{3+}$  ( $\text{C}_{23}\text{H}_{22}\text{N}_6\text{Ru}$ ;  $m/z = 161.365$ ) even at three digits (Figure S12).

X-ray absorption near-edge structure (XANES) measurements were performed for **2** in the solid state and for **3** and **5** in the solution (Figure S13). In the XANES spectrum of **2**, the energy of the Ru-K edge ( $E_{\text{Ru-K}}$ ) was observed at 22119.8 eV, and  $E_{\text{Ru-K}}$  for **3**, formed in situ by addition of 1 equiv of CAN to the aqueous solution of **2**, was observed at 22121.5 eV. Also, with further addition of 2 equiv of CAN,  $E_{\text{Ru-K}}$  for **5** was observed at 22124.0 eV. This high-energy shift indicates the high valency of the Ru center in **5** relative to  $\text{Ru}^{\text{II}}$  for **2** and  $\text{Ru}^{\text{III}}$  for **3**, supporting the assignment of **5** as the +V oxidation state.

The Evans method<sup>40</sup> based on  $^1\text{H}$  NMR spectroscopy was applied to the solution of **5** in  $\text{D}_2\text{O}$  at 277 K and pD 2.9.<sup>41</sup> The

effective magnetic moment ( $\mu_{\text{eff}}$ ) of **5** was calculated to be 2.02 (Figure S14). This value allowed us to determine the spin state of **5** to be  $S = 1/2$  (calculated spin-only  $\mu_{\text{eff}}$ : 1.73). Thus, the Ru center of **5** was assigned to be in the low-spin configuration of the +V oxidation state.

An IR spectrum of the solid sample of **5**, which was obtained with addition of KPF<sub>6</sub> to the aqueous solution of **5**, was measured in the KBr pellet to observe a signal at 875 cm<sup>-1</sup>, assignable to the Ru=N stretching band (Figures 4 and S15).

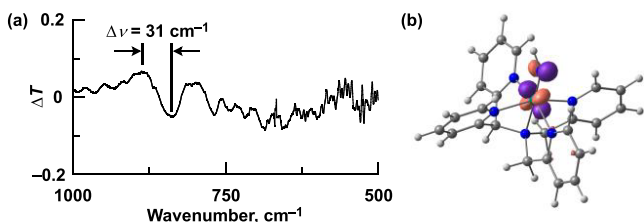
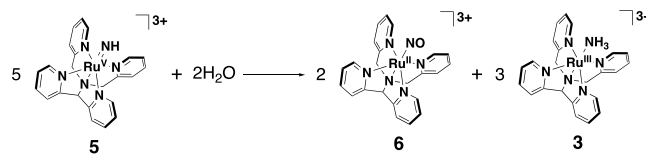


**Figure 4.** (a) Differential IR spectrum of (**5**-<sup>15</sup>N) – (**5**-<sup>14</sup>N) in KBr pellets at room temperature. (b) A DFT-optimized structure with SOMO.

The corresponding band of the <sup>15</sup>N-labeled **5** shifted to 844 cm<sup>-1</sup>, and the isotope shift width ( $\Delta\nu = 31$  cm<sup>-1</sup>; Figure 4a) matched with the calculated value ( $\Delta\nu = 27$  cm<sup>-1</sup>). The value of the Ru–N stretching band is close to that of Ru<sup>VI</sup>–tosyl–imido complexes ( $\nu_{\text{Ru=NR}} = 900\text{--}920$  cm<sup>-1</sup>)<sup>42</sup> and a Ru<sup>V</sup>–oxo complex ( $\nu_{\text{Ru=O}} = 872$  cm<sup>-1</sup>),<sup>43</sup> and thus, the Ru–N bond of **5** should bear a double-bond character. Furthermore, the vibrational analysis of the DFT-optimized structure (Figure 4b) in the doublet state ( $S = 1/2$ ) indicated the stretching energy of the Ru<sup>V</sup>=NH bond to be  $\nu_{\text{calcd}} = 873$  cm<sup>-1</sup>, which was consistent with the experimental value obtained from the IR spectrum. DFT calculations on **5** also suggested that the doublet state is more stable by 9.5 kcal mol<sup>-1</sup> than the corresponding quartet state ( $S = 3/2$ ), which is in Ru<sup>IV</sup>–(N<sup>•-</sup>)–H form bearing the Mayer bond order of 0.83 for the Ru–N bond (Figure S16). The length of the Ru<sup>V</sup>=NH bond in the doublet state of **5** was estimated to be 1.743 Å (Figure 4b); the Mayer bond order was calculated to be 1.67 (Figure S16). Thus, we confirmed the double-bond character of the Ru<sup>V</sup>=NH bond in **5**. In addition, an absorption band assigned to the N–D stretching vibration was observed at  $\nu = 2493$  cm<sup>-1</sup> in the IR spectrum of deuterated **5** (Figure S17b). On the other hand, in the IR spectrum of **5**, no clear N–H band was observed in the range of  $\nu = 2800\text{--}3600$  cm<sup>-1</sup> (Figure S17a and c), since a broad band probably derived from water molecules was observed in the region.

**Self-Decomposition of 5.** To confirm the stability of **5**, the solution of **5** in D<sub>2</sub>O, whose pD was adjusted to 2.5<sup>35</sup> by addition of HClO<sub>4</sub> aq, was stirred at 277 K for 24 h. At this stage, the imido H of **5** should be exchanged with deuterium from D<sub>2</sub>O due to the stronger Lewis acidity of the Ru(V) center. After addition of H<sub>2</sub>Q (0.5 mol equiv), the <sup>1</sup>H NMR spectrum of the solution was measured. Signals derived from deuterated **1**, deuterated **2**, [Ru(N4Py)(NO)]<sup>3+</sup> (**6**),<sup>39</sup> and benzoquinone derived from oxidation of H<sub>2</sub>Q were observed (Figure S18). The concentration ratios of the Ru complexes were determined based on an internal standard of DSS to be 1/2/6 = 32:23:45. Complex **1** in the solution was probably formed through a ligand exchange of **2** in the course of the reduction. Thus, the decomposition reaction of **5** is assumed to be as shown in Scheme 6, where complex **5** reacts with a D<sub>2</sub>O

### Scheme 6. Decomposition Reaction of **5** in Water



molecule at first, and the Ru<sup>III</sup>–hydroxylamine complex<sup>23c</sup> formed is reoxidized by remaining **5** to afford **6**, concomitant with **3**, which should be deuterated in D<sub>2</sub>O as **3** (Scheme 6). Complex **3** formed was reduced with H<sub>2</sub>Q to be **2**.

UV–vis spectral change for the self-decomposition of **5** was also monitored in D<sub>2</sub>O from 0 to 1.0 × 10<sup>5</sup> s (Figure 5). The

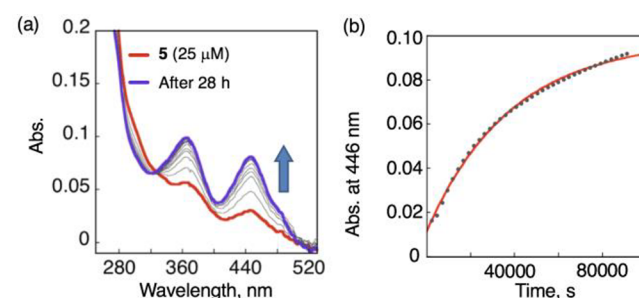


**Figure 5.** UV–vis spectral change (a) and absorbance change at 446 nm (b) for self-decomposition of **5** (25 μM) in D<sub>2</sub>O (pD 2.5) at 277 K.

spectral change accompanied one clear isosbestic point at 330 nm, indicating that the self-decomposition reaction proceeds without any side reactions. Analysis of the absorbance change at 446 nm with the first-order kinetics allowed us to determine  $k_{\text{dec}}$  in D<sub>2</sub>O as  $(2.62 \pm 0.08) \times 10^{-5}$  s<sup>-1</sup>.

**Substrate Oxidation with 5.** We also investigated the reactivity of **5** in quantitative oxidation of organic substrates in acidic water at 277 K. As substrates, 2-propanol (BDE<sub>C–H</sub> = 90.0 kcal mol<sup>-1</sup>),<sup>44</sup> benzyl alcohol (BnOH; BDE<sub>C–H</sub> = 87.5 kcal mol<sup>-1</sup>),<sup>44</sup> and sodium ethylbenzene-sulfonate (EBS; BDE<sub>C–H</sub> = 85.4 kcal mol<sup>-1</sup>)<sup>44</sup> were employed (Table 1).<sup>45</sup> To a solution of **5** in D<sub>2</sub>O (0.15 mM, pD 2.9) was added an excess amount of 2-propanol at 277 K in the presence of NaClO<sub>4</sub> (50 mM) to adjust the ionic strength to be the same as the ionic substrates. After the mixture was stirred for 24 h, the product was identified to be solely acetone using <sup>1</sup>H NMR spectroscopy (Figure S20b) and the yield of acetone was determined to be 77% based on **5**. After the oxidation reaction, no signals assignable to the Ru species were observed except for small peaks of **6**, and the yield of **6** based on **2** was determined to be 9%. However, upon addition of 0.5 mol equiv of H<sub>2</sub>Q as a reductant to the solution, the distinctive signals of **2** were observed in the diamagnetic region and the recovery yield of **2** was 91% (Figure S20c). This ratio can be accounted for by the competition between the oxidation of 2-propanol by **5** (eq 1) and reaction of **5** with solvent water (eq 2; see also Scheme 5).<sup>23c</sup>

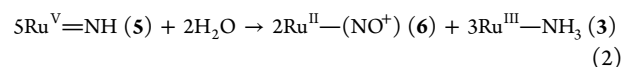
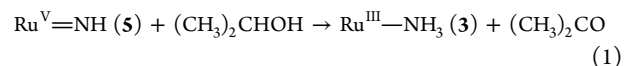
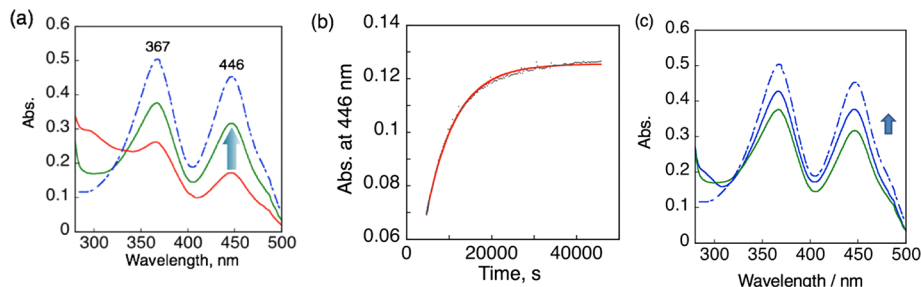


Table 1. Summary of Second-Order Rate Constants for Substrate Oxidation by 5

substrate	product	$k_{C-H}^a$	$k_{C-D}^a$	$k_{D_2O}^a$	$k_{C-H}/k_{C-D}$	$k_{C-H}/k_{D_2O}$
EBS	HEBS	$(8.6 \pm 0.4) \times 10^{-3}$	$(4.5 \pm 0.5) \times 10^{-4}$	$(1.9 \pm 0.1) \times 10^{-4}$	19	45
2-propanol	acetone	$(2.5 \pm 0.2) \times 10^{-3}$	$(1.03 \pm 0.04) \times 10^{-3}$	$(8.4 \pm 0.9) \times 10^{-3}$	2.4	3.0
benzyl alcohol	benzaldehyde	$(8.4 \pm 0.4) \times 10^{-3}$	$(6.4 \pm 0.5) \times 10^{-4}$	$(7.8 \pm 0.9) \times 10^{-4}$	13	17

<sup>a</sup>Units of  $M^{-1} s^{-1}$ .



**Figure 6.** (a) UV-vis spectral change for oxidation of EBS (10.7 mM) by 5 (25  $\mu$ M) in  $H_2O$  (pH 2.5) at 277 K: UV-vis spectrum of 2 (blue dot-dash line), 5 formed in situ by addition of 3 equiv of CAN to 2 (red solid line), and after addition of EBS and stirring for 14 h (green solid line). (b) The absorbance change at 446 nm (black dots) and the curve fitting based on the pseudo-first-order kinetics (red solid line). (c) UV-vis spectrum after addition of  $H_2Q$  (12.5  $\mu$ M) to the reaction mixture of EBS oxidation with 5: UV-vis spectrum of 2 (blue dot-dash line), after addition of EBS to the solution of 5 with stirring for 14 h (green solid line), and after further addition of 0.5 mol equiv of  $H_2Q$  to the reaction mixture (blue solid line).

Consequently, 77% of 5 was used to oxidize 2-propanol to form 3 in 77% yield as in eq 1; 23% of 5 was consumed in the reaction with a water molecule to give 9% and 14% yields of 6 and 3, respectively, as in eq 2. Thereby, 91% yield of 3 in total was obtained from the reaction. In light of the yields of the products, the stoichiometry of the reactions was fully consistent with eqs 1 and 2. Thus, we can conclude that complex 5 can abstract C–H hydrogen atoms from organic substrates without any *N*-rebound process as reported for high-valent  $M\equiv N$  and  $M=NR$  complexes so far.<sup>46</sup> Note that the  $Ru^V=NH$  complex 5 apparently accepts two hydrogen atoms ( $2H^+ + 2e^-$ ) from the substrate to form the  $Ru^{III}-NH_3$  complex 3 and that the Ru center holds the nitrogen as a proton-accepting site in the course of the oxidation reaction. Also, BnOH and EBS were subjected to quantitative oxidation by 5 in  $D_2O$  at pD 2.9, and the products were identified by  $^1H$  NMR spectroscopy to be benzaldehyde and sodium 1-hydroxyethyl-benzene-sulfonate (HEBS), respectively (Figure S21a and b). The yields were calculated to be 90% for benzaldehyde and 90% for HEBS. The product from EBS was not sodium 1-aminoethylbenzene-sulfonate but HEBS, and thus, the amido ligand in the  $Ru^{IV}-NH_2$  complex possibly formed from 5 through hydrogen-atom abstraction without the *N*-rebound process.<sup>46</sup>

When cyclobutanol was oxidized by 5 in  $D_2O$ , whose pD was adjusted to 2.9 at 277 K, cyclobutanone was solely observed as the product in the  $^1H$  NMR spectrum (Figure S22a) in 17% yield on the basis of 5.<sup>47</sup> In stark contrast,  $[Ru^{IV}(O)(N_4Py)(OH_2)]^{2+28c}$  was employed as an oxidant for cyclobutanol oxidation to afford a complicated mixture of ring-opening products. The mixture should be formed from the cyclobutanol radical produced via hydrogen-atom transfer to the  $Ru^{IV}=O$  complex (Figure S22b).<sup>48</sup> Therefore, it has been clearly indicated that the C–H oxidation by 5 proceeds not through a hydrogen-atom abstraction mechanism but through a hydride-transfer mechanism.<sup>48</sup> The hydride-transfer reaction affords a carbo-cation derived from a substrate and the corresponding  $Ru^{III}-NH_2$  complex from 5; the carbocation

undergoes nucleophilic attack of a water molecule to afford the corresponding alcohol or ketone derivative (Scheme 2b).

**Kinetic Studies on the Substrate Oxidation by 5.** Kinetic analysis was performed for the EBS oxidation reaction by 5 in acidic water at 277 K. To an aqueous solution of 5 (25  $\mu$ M), whose pH was adjusted to 2.5 by addition of  $HClO_4$  aq, was added an excess amount of EBS (11–64 mM) at 277 K to provide pseudo-first-order reaction conditions. Progress of the reactions was monitored by UV-vis spectroscopy, and absorbance increases were observed at 365 and 446 nm, derived from the formation of 3 (Figure 6a). After the reaction, 0.5 mol equiv of  $H_2Q$  was added to reduce complex 3 formed, and the absorption bands at 365 and 446 nm were further recovered to 83% of the original absorbance of 2 (Figure 6c). Time-courses of the absorbance change at 446 nm were analyzed to determine the pseudo-first-order rate constants ( $k_{obs}$ ) (Figure 6b), and the  $k_{obs}$  values showed a linear relationship against the concentration of EBS, allowing us to determine the second-order rate constant ( $k_{C-H}$ ) to be  $(8.6 \pm 0.4) \times 10^{-3} M^{-1} s^{-1}$  (filled circles and red lines in Figure 7). Additionally, the intercept of the linear fitting for the EBS

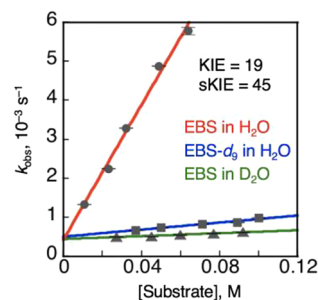


**Figure 7.** Dependence of pseudo-first-order rate constant for EBS oxidation by 5 on the substrate concentration: filled circles and red solid line for EBS oxidation in  $H_2O$ , filled squares and blue solid line for EBS- $d_6$  oxidation in  $H_2O$ , and filled triangles and green solid line for EBS oxidation in  $D_2O$ .

oxidation by **5** was determined to be  $(4 \pm 1) \times 10^{-5} \text{ s}^{-1}$ , which was fairly consistent with the self-decomposition rate constant,  $k_{\text{dec}}$   $(2.62 \pm 0.08) \times 10^{-5} \text{ s}^{-1}$  (see above).

The kinetic isotope effect (KIE) in the EBS oxidation reaction by **5** was also investigated using deuterated EBS (EBS- $d_9$ ) as the substrate (Figure 7). In consequence, the second-order rate constant ( $k_{\text{C-D}}$ ) was determined to be  $(4.5 \pm 0.5) \times 10^{-4} \text{ M}^{-1} \text{ s}^{-1}$  (filled squares and blue line in Figure 7), and the  $k_{\text{C-H}}/k_{\text{C-D}}$  value was calculated to be 19 (Table 1). Therefore, the oxidation reaction of EBS by **5** involves C–H abstraction in the rate-determining process. In addition, we observed remarkably large solvent KIE; oxidation of EBS by **5** was performed in buffered  $\text{D}_2\text{O}$  (pD 2.9) (filled triangles and green line in Figure 7), and the second-order rate constant,  $k_{\text{D}_2\text{O}}$ , was determined to be  $(1.9 \pm 0.1) \times 10^{-4} \text{ M}^{-1} \text{ s}^{-1}$ . Thus, the solvent KIE  $k_{\text{C-H}}/k_{\text{D}_2\text{O}}$  was determined to be 45 (Table 1). Such a large solvent KIE has never been reported for the reactions of any metal–oxo complexes.<sup>49,50</sup>

Oxidation reactions of 2-propanol and BnOH by **5** were also kinetically analyzed under pseudo-first-order conditions to determine the  $k_{\text{obs}}$  values (Figures S23 and S24). In these studies,  $\text{NaClO}_4$  (50 mM) was added to the reaction mixture to unify the ionic strength to the case of EBS.<sup>51</sup> UV–vis spectral changes observed during the oxidation reactions were similar to that for EBS oxidation, as shown in Figure 6a, and the apparent rate constants,  $k_{\text{obs}}$ , were obtained on the basis of the absorbance changes at 446 nm. Dependence of the  $k_{\text{obs}}$  values on the substrate concentrations provided the second-order rate constants ( $k_{\text{C-H}}$ ) as  $(2.5 \pm 0.2) \times 10^{-3} \text{ M}^{-1} \text{ s}^{-1}$  for 2-propanol and  $(8.4 \pm 0.4) \times 10^{-3} \text{ M}^{-1} \text{ s}^{-1}$  for BnOH (Table 1). In addition, deuterated 2-propanol (2-propanol- $d_8$ ) and di-deuterated BnOH at the benzylic position (BnOH- $d_2$ ) were subjected to the oxidation by **5** to determine the second-order rate constants ( $k_{\text{C-D}}$ ). As a result of pseudo-first-order kinetic analysis with these deuterated substrates,  $k_{\text{C-D}}$  values were determined to be  $(1.03 \pm 0.04) \times 10^{-3} \text{ M}^{-1} \text{ s}^{-1}$  for 2-propanol- $d_8$  and  $(6.4 \pm 0.5) \times 10^{-4} \text{ M}^{-1} \text{ s}^{-1}$  for BnOH- $d_2$ . Thereby, the  $k_{\text{C-H}}/k_{\text{C-D}}$  values were 2.4 for 2-propanol and 13 for BnOH. Solvent KIEs for 2-propanol and BnOH were also investigated in  $\text{D}_2\text{O}$  (pD 2.9) in the presence of  $\text{NaClO}_4$  (50 mM). Consequently, the second-order rate constants ( $k_{\text{D}_2\text{O}}$ ) were determined to be  $(8.4 \pm 0.9) \times 10^{-3} \text{ M}^{-1} \text{ s}^{-1}$  for 2-propanol and  $(7.8 \pm 0.9) \times 10^{-4} \text{ M}^{-1} \text{ s}^{-1}$  for BnOH, and thus, the  $k_{\text{C-H}}/k_{\text{D}_2\text{O}}$  values were 3 for 2-propanol and 17 for BnOH.

C–H oxidation proceeding through hydrogen-atom (H•) abstraction is known to show a linear relationship between bond dissociation energy (BDE) of substrates and logarithms of the rate constants, i.e., the Bell–Evans–Polanyi (BEP) plot.<sup>52</sup> Therefore, we have provided a BEP plot for C–H oxidation by **5** on the basis of the second-order rate constants ( $k_{\text{C-H}}$ ) of the oxidations of EBS, BnOH, and 2-propanol. The rate constants were normalized by dividing with the number of the equivalent hydrogen atoms to be abstracted.<sup>52</sup> The BEP plot does not show a linear relationship between the BDE values and logarithms of the normalized  $k_{\text{C-H}}$  values (Figure S27), suggesting that complex **5** does not perform C–H oxidation of organic substrates through a hydrogen-atom abstraction mechanism.

**A Plausible Reaction Mechanism of Substrate Oxidation by 5.** Based on the kinetic studies on the substrate oxidation by **5** and the result of cyclobutanol oxidation by **5** to afford cyclobutanone selectively, we propose the rate-determining step involves not only hydride transfer from a

C–H bond of an organic substrate but also proton transfer from a water molecule as the solvent (Figure 8). To confirm

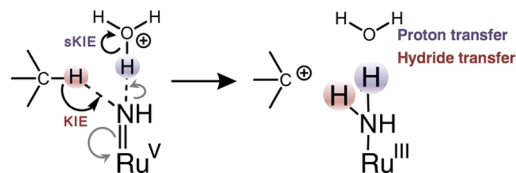


Figure 8. Concerted hydride and proton transfer to **5**.

this hypothesis, we have conducted theoretical studies on the reaction mechanism of the substrate oxidation by **5**. At first, the reaction profile for the cyclobutanol oxidation by **5** was obtained by DFT calculations using a polarizable continuum model (PCM) method<sup>53</sup> to include solvation effects of water in the calculations (Figure 9). In the calculations, we included

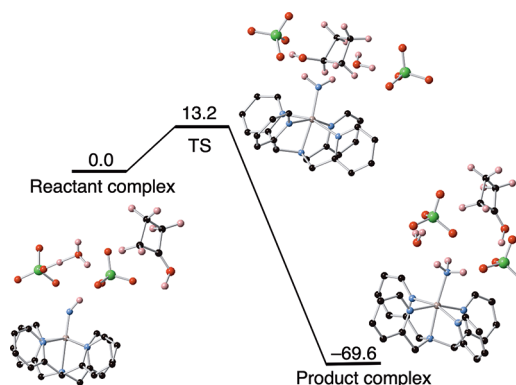
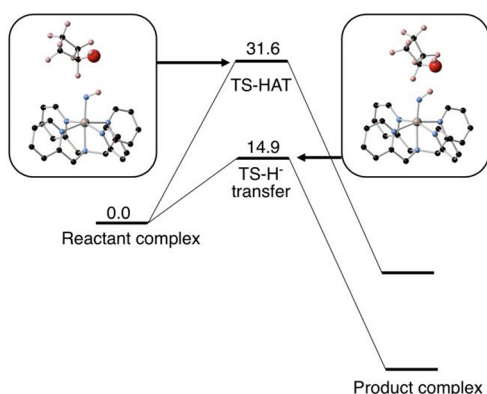


Figure 9. Reaction profile for cyclobutanol oxidation by **5** based on DFT calculations.

the cationic part of **5**,  $[\text{Ru}^{\text{V}}(\text{NH})(\text{N4Py})]^{3+}$ , two  $\text{ClO}_4^-$  ions as the counteranion, one cyclobutanol molecule, and one oxonium ion ( $\text{H}_3\text{O}^+$ ) as a proton source derived from the solvent under acidic conditions. In the calculated transition state, the imide nitrogen strongly interacts both with the hydrogen atom attached to the hydroxy-substituted carbon in cyclobutanol and a proton of the oxonium ion. Then, the Ru–N bond bears the single-bond character. Finally, the reaction affords the corresponding  $\text{Ru}^{\text{III}}\text{—NH}_3$  complex, **3**, and a carbocation derivative of cyclobutanol, which immediately afford cyclobutanone through deprotonation from the OH group. The calculated activation energy to reach the transition state is  $13.2 \text{ kcal mol}^{-1}$ . Therefore, this reaction can proceed through a hydride-transfer mechanism even at ambient temperature.

In addition, the calculated activation energy for the cyclobutanol oxidation through the hydride-transfer mechanism was compared to that through a hydrogen-atom transfer mechanism. In the calculations,  $\text{ClO}_4^-$  ions and the oxonium ion were not included (Figure 10). The activation barrier involving the hydride transfer mechanism to give the  $\text{Ru}^{\text{III}}\text{—NH}_2$  complex and the carbocation derivative of cyclobutanol was  $14.9 \text{ kcal mol}^{-1}$ , whereas that through the hydrogen-atom abstraction mechanism to give the  $\text{Ru}^{\text{IV}}\text{—NH}_2$  complex and hydroxy-cyclobutyl radical was  $31.6 \text{ kcal mol}^{-1}$ . Therefore, as for the C–H oxidation by **5**, the hydride-transfer mechanism is highly favorable in comparison with the hydrogen-atom abstraction mechanism.<sup>54</sup> This can be explained on the basis



**Figure 10.** Comparison of activation barriers for the hydride-transfer mechanism and hydrogen-atom abstraction mechanism for oxidation of cyclobutanol by **5**. The units in relative energies are kcal mol<sup>-1</sup>.

of the fact that the Ru<sup>IV</sup>—NH<sub>2</sub> complex **4** that should be formed in the hydrogen-atom abstraction is unstable and easily disproportionate into complexes **3** and **5** (see above). Due to the instability of **4**, the substrate oxidation by **5** avoids the hydrogen-atom (H•) abstraction pathway and thus proceeds through hydride transfer.

## CONCLUSION

A Ru<sup>V</sup>=NH complex, **5**, having N4Py as an ancillary pentadentate ligand, was formed through the PCET oxidation of the corresponding Ru<sup>II</sup>—ammine complex **2** in acidic water at 277 K without formation of the undesired nitrosyl complex, **6**. Complex **5** was characterized with HR-ESI-TOF-MS spectrometry and <sup>1</sup>H NMR, IR, and X-ray absorption spectroscopies as [Ru<sup>V</sup>(NH)(N<sub>4</sub>Py)]<sup>3+</sup> in the S = 1/2 spin state. Complex **5** performs C—H oxidation of organic substrates, such as 2-propanol, and gives acetone and the corresponding Ru<sup>III</sup>—ammine complex, **3**, with showing complete stoichiometry. The conspicuous difference in the reactivity between the Ru<sup>IV</sup>—oxo complexes and the Ru<sup>V</sup>=NH complex **5** revealed herein is that complex **5** affords the corresponding Ru<sup>III</sup>—NH<sub>3</sub> complex as the product after 2e<sup>-</sup> oxidation of a substrate without performing the nitrogen-rebound process. Cyclobutanol oxidation by **5** afforded cyclobutanone as the sole product, indicating that the C—H oxidation by **5** proceeds not through hydrogen-atom transfer but instead through the hydride-transfer mechanism, which is also supported by DFT calculations. In addition, large C—H KIE and solvent KIE, as revealed by kinetic studies, indicate that hydride transfer from the substrate and proton transfer from water as the solvent are involved in the rate-determining step of the C—H oxidation by **5** through the nitrogen-non-rebound mechanism.

## ASSOCIATED CONTENT

### Supporting Information

The Supporting Information is available free of charge on the ACS Publications website at DOI: 10.1021/acs.inorgchem.9b01781.

Synthetic details, <sup>1</sup>NMR, UV—vis, and ESI-TOF-MS spectra, voltammograms, UV—vis spectral changes for kinetic studies, and computational details (PDF)

## Accession Codes

CCDC 1906718 contains the supplementary crystallographic data for this paper. These data can be obtained free of charge via [www.ccdc.cam.ac.uk/data\\_request/cif](http://www.ccdc.cam.ac.uk/data_request/cif), or by emailing [data\\_request@ccdc.cam.ac.uk](mailto:data_request@ccdc.cam.ac.uk), or by contacting The Cambridge Crystallographic Data Centre, 12 Union Road, Cambridge CB2 1EZ, UK; fax: +44 1223 336033.

## AUTHOR INFORMATION

### Corresponding Author

\*E-mail: [kojima@chem.tsukuba.ac.jp](mailto:kojima@chem.tsukuba.ac.jp)

### ORCID

Tomoya Ishizuka: 0000-0002-3897-026X

Hiroaki Kotani: 0000-0001-7737-026X

Shin-ichi Adachi: 0000-0002-3676-1165

Kentaro Yamaguchi: 0000-0002-2629-716X

Kazunari Yoshizawa: 0000-0002-6279-9722

Takahiko Kojima: 0000-0001-9941-8375

### Notes

The authors declare no competing financial interest.

## ACKNOWLEDGMENTS

This work was supported by Grants-in-Aid (15H00915, 17H03027, 17H06438) from the Japan Society of the Promotion of Science of Japan (JSPS) and a grant (JPMJCR16P1) through CREST (Japan Science and Technology Agency). T.K. appreciates financial support from The Mitsubishi Foundation. A JSPS research fellowship for young scientists (26-2445) to M.M. is also appreciated.

## REFERENCES

- (a) Meunier, B.; de Visser, S. P.; Shaik, S. Mechanism of Oxidation Reactions Catalyzed by Cytochrome P450 Enzymes. *Chem. Rev.* **2004**, *104*, 3947. (b) Denisov, I. G.; Makris, T. M.; Sligar, S. G.; Schlichting, I. Structure and Chemistry of Cytochrome P450. *Chem. Rev.* **2005**, *105*, 2253. (c) Baik, M.-H.; Newcomb, M.; Friesner, R. A.; Lippard, S. J. Mechanistic Studies on the Hydroxylation of Methane by Methane Monooxygenase. *Chem. Rev.* **2003**, *103*, 2385.
- (a) Costas, M.; Mehn, M. P.; Jensen, M. P.; Que, L., Jr. Dioxygen Activation at Mononuclear Nonheme Iron Active Sites: Enzymes, Models, and Intermediates. *Chem. Rev.* **2004**, *104*, 939. (b) Gagliardi, C. J.; Westlake, B. C.; Kent, C. A.; Paul, J. J.; Papanikolas, J. M.; Meyer, T. J. Integrating Proton Coupled Electron Transfer (PCET) and Excited States. *Coord. Chem. Rev.* **2010**, *254*, 2459.
- (a) Meyer, T. J.; Huynh, V. The Remarkable Reactivity of High Oxidation State Ruthenium and Osmium Polypyridyl Complexes. *Inorg. Chem.* **2003**, *42*, 8140. (b) Nugent, W. A.; Mayer, J. M. *Metal-Ligand Multiple Bonds*; John Wiley & Sons: New York, 1988. (c) Eikey, R. A.; Abu-Omar, M. M. Nitrido and Imido Transition Metal Complexes of Groups 6–8. *Coord. Chem. Rev.* **2003**, *243*, 83.
- (a) Scepianiak, J. J.; Vogel, C. S.; Khusniyarov, M. M.; Heinemann, F. W.; Meyer, K.; Smith, J. M. Synthesis, Structure, and Reactivity of an Iron(V) Nitride. *Science* **2011**, *331*, 1049. (b) Berry, J. F.; Bill, E.; Bothe, E.; George, S. D.; Mienert, B.; Neese, F.; Wieghardt, K. An Octahedral Coordination Complex of Iron(VI). *Science* **2006**, *312*, 1937.
- (a) Scheibel, M. G.; Askevold, B.; Heinemann, F. W.; Reijerse, E. J.; de Bruin, B.; Schneider, S. Closed-shell and Open-shell Square-planar Iridium Nitrido Complexes. *Nat. Chem.* **2012**, *4*, 552.
- (a) Man, W.-L.; Tang, T.-M.; Wong, T.-W.; Lau, T.-C.; Peng, S.-M.; Wong, W.-T. Highly Electrophilic (Salen)ruthenium(VI) Nitrido Complexes. *J. Am. Chem. Soc.* **2004**, *126*, 478.
- (a) Wang, D.; Loose, F.; Chirik, P. J.; Knowles, R. R. N-H Bond Formation in a Manganese(V) Nitride Yields Ammonia by Light-

Driven Proton-Coupled Electron Transfer. *J. Am. Chem. Soc.* **2019**, *141*, 4795.

(8) (a) Du Bois, J.; Tomooka, C. S.; Hong, J.; Carreira, E. M. Nitridomanganese(V) Complexes: Design, Preparation, and Use as Nitrogen Atom-Transfer Reagents. *Acc. Chem. Res.* **1997**, *30*, 364.

(b) Man, W.-L.; Lam, W. W. Y.; Lau, T.-C. Reactivity of Nitrido Complexes of Ruthenium(VI), Osmium(VI), and Manganese(V) Bearing Schiff Base and Simple Anionic Ligands. *Acc. Chem. Res.* **2014**, *47*, 427.

(9) (a) Man, W.-L.; Lam, W. W. Y.; Kwong, H.-K.; Peng, S.-M.; Wong, W.-T.; Lau, T.-C. Reaction of a (Salen)ruthenium(VI) Nitrido Complex with Thiols. C-H Bond Activation by (Salen)ruthenium(IV) Sulfilamido Species. *Inorg. Chem.* **2010**, *49*, 73. (b) Man, W.-L.; Lam, W. W. Y.; Kwong, H.-K.; Yiu, S.-M.; Lau, T.-C. Ligand-Accelerated Activation of Strong C-H Bonds of Alkanes by a (Salen)ruthenium(VI)-Nitrido Complex. *Angew. Chem., Int. Ed.* **2012**, *51*, 9101.

(10) (b) Müller, P.; Fruit, C. Enantioselective Catalytic Aziridinations and Asymmetric Nitrene Insertions into CH Bonds. *Chem. Rev.* **2003**, *103*, 2905. (a) Che, C.-M.; Lo, V. K.-Y.; Zhou, C.-Y. 7.02 Oxidation by Metals (Nitrene). *Comprehensive Organic Synthesis II* **2014**, 26–85.

(11) (a) Davies, H. M. L.; Manning, J. R. Catalytic C-H Functionalization by Metal Carbenoid and Nitrenoid Insertion. *Nature* **2008**, *451*, 417. (b) Collet, F.; Dodd, R. H.; Dauban, P. Catalytic C-H Amination: Recent Progress and Future Directions. *Chem. Commun.* **2009**, 5061. (c) Lu, H.; Zhang, X. P. Catalytic C-H Functionalization by Metalloporphyrins: Recent Developments and Future Directions. *Chem. Soc. Rev.* **2011**, *40*, 1899.

(12) Cowley, R. E.; Eckert, N. A.; Vaddadi, S.; Figg, T. M.; Cundari, T. R.; Holland, P. L. Selectivity and Mechanism of Hydrogen Atom Transfer by an Isolable Imidoiron(III) Complex. *J. Am. Chem. Soc.* **2011**, *133*, 9796.

(13) (a) Hennessy, E. T.; Betley, T. A. Complex N-Heterocycle Synthesis via Iron-Catalyzed, Direct C-H Bond Amination. *Science* **2013**, *340*, 591. (b) Iovan, D. A.; Betley, T. A. Characterization of Iron-Imido Species Relevant for N-Group Transfer Chemistry. *J. Am. Chem. Soc.* **2016**, *138*, 1983. (c) Wilding, M. J. T.; Iovan, D. A.; Betley, T. A. High-Spin Iron Imido Complexes Competent for C-H Bond Amination. *J. Am. Chem. Soc.* **2017**, *139*, 12043.

(14) Bucinsky, L.; Breza, M.; Lee, W.-T.; Hickey, A. K.; Dickie, D. A.; Nieto, I.; DeGayner, J. A.; Harris, T. D.; Meyer, K.; Krzystek, J.; Ozarowski, A.; Nehr Korn, J.; Schnegg, A.; Holldack, K.; Herber, R. H.; Telsler, J.; Smith, J. M. Spectroscopic and Computational Studies of Spin States of Iron(IV) Nitrido and Imido Complexes. *Inorg. Chem.* **2017**, *56*, 4751.

(15) (a) Bräse, S.; Gil, C.; Knepper, K.; Zimmermann, V. Organic Azides: An Exploding Diversity of a Unique Class of Compounds. *Angew. Chem., Int. Ed.* **2005**, *44*, 5188. (b) Cenini, S.; Gallo, E.; Caselli, A.; Ragaini, F.; Fantauzzi, S.; Piangiolino, C. Coordination Chemistry of Organic Azides and Amination Reactions Catalyzed by Transition Metal Complexes. *Coord. Chem. Rev.* **2006**, *250*, 1234.

(16) (a) Eckert, N. A.; Vaddadi, S.; Lachicotte, S. J.; Cundari, T. R.; Holland, P. L.; Stoian, S. Coordination-Number Dependence of Reactivity in an Imidoiron(III) Complex. *Angew. Chem., Int. Ed.* **2006**, *45*, 6868. (b) Cowley, R. E.; DeYonker, N. J.; Eckert, N. A.; Cundari, T. R.; DeBeer, S.; Bill, E.; Ottenwaelder, X.; Flaschenriem, C.; Holland, P. L. Three-Coordinate Terminal Imidoiron(III) Complexes: Structure, Spectroscopy, and Mechanism of Formation. *Inorg. Chem.* **2010**, *49*, 6172. (c) Abu-Omar, M. M.; Shields, C. E.; Edwards, N. Y.; Eikey, R. A. On the Mechanism of the Reaction of Organic Azides with Transition Metals: Evidence for Triplet Nitrene Capture. *Angew. Chem., Int. Ed.* **2005**, *44*, 6203.

(17) (a) Zdilla, M. J.; Abu-Omar, M. M. Mechanism of Catalytic Aziridination with Manganese Corrole: The Often Postulated High-Valent Mn(V) Imido Is Not the Group Transfer Reagent. *J. Am. Chem. Soc.* **2006**, *128*, 16971. (b) Bagchi, V.; Paraskevopoulou, P.; Das, P.; Chi, L.; Wang, Q.; Choudhury, A.; Mathieson, J. S.; Cronin, L.; Pardue, D. B.; Cundari, T. R.; Mitrikas, G.; Sanakis, Y.; Stavropoulos, P. A Versatile Tripodal Cu(I) Reagent for C-N Bond

Construction via Nitrene-Transfer Chemistry: Catalytic Perspectives and Mechanistic Insights on C-H Aminations/Amidations and Olefin Aziridinations. *J. Am. Chem. Soc.* **2014**, *136*, 11362. (c) Roizen, J. L.; Harvey, N. E.; Du Bois, J. Metal-Catalyzed Nitrogen-Atom Transfer Methods for the Oxidation of Aliphatic C-H Bonds. *Acc. Chem. Res.* **2012**, *45*, 911.

(18) (a) King, D. M.; McMaster, J.; Tuna, F.; McInnes, E. J. L.; Lewis, W.; Blake, A. J.; Liddle, S. T. Synthesis and Characterization of an f-Block Terminal Imido [U = NH] Complex: A Masked Uranium(IV) Nitride. *J. Am. Chem. Soc.* **2014**, *136*, 5619. (b) McKarns, P. J.; Yap, G.; Rheingold, A. L.; Winter, C. H. Synthesis, Structure, and Characterization of the Hydrogen-Substituted Imido Complex  $\text{TiCl}_2(\text{NH})(\text{OPPh}_3)_2$ . *Inorg. Chem.* **1996**, *35*, 5968. (c) Lutz, C. M.; Wilson, S. R.; Shapley, P. A. The First Imido Complex of Osmium(VI),  $[\text{CpOs}(\text{NH})(\text{CH}_2\text{SiMe}_3)_2]\text{[SO}_3\text{CF}_3]$ . *Organometallics* **2005**, *24*, 3350.

(19) Grant, L. N.; Pinter, B.; Gu, J.; Mindiola, D. J. Molecular Zirconium Nitride Super Base from a Mononuclear Parent Imide. *J. Am. Chem. Soc.* **2018**, *140*, 17399.

(20) Warren, J. J.; Tronic, T. A.; Mayer, J. M. Thermochemistry of Proton-Coupled Electron Transfer Reagents and its Implications. *Chem. Rev.* **2010**, *110*, 6961.

(21) (a) Bezdek, M. J.; Chirik, P. J. Interconversion of Molybdenum Imido and Amido Complexes by Proton-Coupled Electron Transfer. *Angew. Chem., Int. Ed.* **2018**, *57*, 2224. (b) Milsmann, C.; Semproni, S. P.; Chirik, P. J. N-N Bond Cleavage of 1,2-Diaryldiazines and N-H Bond Formation via H-Atom Transfer in Vanadium Complexes Supported by a Redox-Active Ligand. *J. Am. Chem. Soc.* **2014**, *136*, 12099.

(22) (a) Huynh, M. H. V.; White, P. S.; John, K. D.; Meyer, T. J. Isolation and Characterization of the Osmium(V)-Imido Complex  $[\text{OsV}(\text{Tp})(\text{Cl})_2(\text{NH})]$ . *Angew. Chem., Int. Ed.* **2001**, *40*, 4049. (b) Yandulov, D. V.; Schrock, R. R. Studies Relevant to Catalytic Reduction of Dinitrogen to Ammonia by Molybdenum Triamidoamine Complexes. *Inorg. Chem.* **2005**, *44*, 1103.

(23) (a) Thompson, M. S.; Meyer, T. J. Oxidation of Coordinated Ammonia to Nitrate. *J. Am. Chem. Soc.* **1981**, *103*, 5577. (b) Murphy, W. R., Jr.; Takeuchi, K. J.; Meyer, T. J. Interconversion of Nitrite and Ammonia: Progress Toward a Model for Nitrite Reductase. *J. Am. Chem. Soc.* **1982**, *104*, 5817. (c) Murphy, W. R., Jr.; Takeuchi, K. J.; Barley, M. H.; Meyer, T. J. Mechanism of Reduction of Bound Nitrite to Ammonia. *Inorg. Chem.* **1986**, *25*, 1041.

(24) (a) Ishitani, O.; White, P. S.; Meyer, T. J. Formation of Dinitrogen by Oxidation of  $[(\text{bpy})_2(\text{NH}_3)\text{RuORu}(\text{NH}_3)(\text{bpy})_2]^{4+}$ . *Inorg. Chem.* **1996**, *35*, 2167. (b) Ishitani, O.; Ando, E.; Meyer, T. J. Dinitrogen Formation by Oxidative Intramolecular N...N Coupling in *cis,cis*- $[(\text{bpy})_2(\text{NH}_3)\text{RuORu}(\text{NH}_3)(\text{bpy})_2]^{4+}$ . *Inorg. Chem.* **2003**, *42*, 1707.

(25) (a) Groves, J. T.; McClusky, G. A. Aliphatic Hydroxylation via Oxygen Rebound. Oxygen Transfer Catalyzed by Iron. *J. Am. Chem. Soc.* **1976**, *98*, 859. (c) Cho, K.; Leeladee, P.; McGown, A. J.; DeBeer, S.; Goldberg, D. P. A High-Valent Iron-Oxo Corrolazine Activates C-H Bonds via Hydrogen-Atom Transfer. *J. Am. Chem. Soc.* **2012**, *134*, 7392.

(26) (a) Moyer, B. A.; Thompson, M. S.; Meyer, T. J. Chemically Catalyzed Net Electrochemical Oxidation of Alcohols, Aldehydes, and Unsaturated Hydrocarbons Using the System  $(\text{trpy})\text{-Ru}(\text{OH}_2)^{2+}/(\text{trpy})(\text{bpy})\text{RuO}^{2+}$ . *J. Am. Chem. Soc.* **1980**, *102*, 2310. (b) Roecker, L.; Meyer, T. J. Hydride Transfer in the Oxidation of Alcohols by  $[(\text{bpy})_2(\text{py})\text{Ru}(\text{Q})]^{2+}$ . A  $k_{\text{H}}/k_{\text{D}}$  Kinetic Isotope Effect of 50. *J. Am. Chem. Soc.* **1987**, *109*, 746.

(27) (a) Rodríguez, M.; Romero, I.; Llobet, A.; Deronzier, A.; Biner, M.; Parella, T.; Stoeckli-Evans, H. Synthesis, Structure, and Redox and Catalytic Properties of a New Family of Ruthenium Complexes Containing the Tridentate bpea Ligand. *Inorg. Chem.* **2001**, *40*, 4150. (b) Bryant, J. R.; Mayer, J. M. Oxidation of C-H Bonds by  $[(\text{bpy})_2(\text{py})\text{Ru}^{\text{IV}}\text{O}]^{2+}$  Occurs by Hydrogen Atom Abstraction. *J. Am. Chem. Soc.* **2003**, *125*, 10351. (c) Kojima, T.; Nakayama, K.; Ikemura, K.; Ogura, T.; Fukuzumi, S. Formation of a Ruthenium(IV)-Oxo

Complex by Electron-Transfer Oxidation of a Coordinatively Saturated Ruthenium(II) Complex and Detection of Oxygen-Rebound Intermediates in C-H Bond Oxygenation. *J. Am. Chem. Soc.* **2011**, *133*, 11692.

(28) (a) Hirai, Y.; Kojima, T.; Mizutani, Y.; Shiota, Y.; Yoshizawa, K.; Fukuzumi, S. Ruthenium-Catalyzed Selective and Efficient Oxygenation of Hydrocarbons with Water as an Oxygen Source. *Angew. Chem., Int. Ed.* **2008**, *47*, 5772. (b) Kojima, T.; Hirai, Y.; Ishizuka, T.; Shiota, Y.; Yoshizawa, K.; Ikemura, K.; Ogura, T.; Fukuzumi, S. A Low-Spin Ruthenium(IV)-Oxo Complex: Does the Spin State Have an Impact on the Reactivity? *Angew. Chem., Int. Ed.* **2010**, *49*, 8449. (c) Ohzu, S.; Ishizuka, T.; Hirai, Y.; Jiang, H.; Sakaguchi, M.; Ogura, T.; Fukuzumi, S.; Kojima, T. Mechanistic Insight into Catalytic Oxidations of Organic Compounds by Ruthenium(IV)-oxo Complexes with Pyridylamine Ligands. *Chem. Sci.* **2012**, *3*, 3421. (d) Ishizuka, T.; Ohzu, S.; Kotani, H.; Shiota, Y.; Yoshizawa, K.; Kojima, T. Hydrogen Atom Abstraction Reactions Independent of C-H Bond Dissociation Energies of Organic Substrates in Water: Significance of Oxidant-Substrate Adduct Formation. *Chem. Sci.* **2014**, *5*, 1429.

(29) Hammes-Schiffer, S. Comparison of Hydride, Hydrogen Atom, and Proton Coupled Electron Transfer Reactions. *ChemPhysChem* **2002**, *3*, 33.

(30) (a) Man, W.-L.; Lam, W. W. Y.; Kwong, H.-K.; Yiu, S.-M.; Lau, T.-C. Ligand Accelerated Activation of Strong C-H Bonds of Alkanes by a (Salen)ruthenium(VI)-Nitrido Complex. *Angew. Chem., Int. Ed.* **2012**, *51*, 9101. (b) Aguila, M. J. B.; Badiei, Y. M.; Warren, T. H. Mechanistic Insights into C-H Amination via Dicopper Nitrenes. *J. Am. Chem. Soc.* **2013**, *135*, 9399.

(31) (a) Thompson, M. S.; Meyer, T. J. Mechanisms of Oxidation of 2-Propanol by Polypyridyl Complexes of Ruthenium(III) and Ruthenium(IV). *J. Am. Chem. Soc.* **1982**, *104*, 4106. (b) Al-Ajlouni, A. M.; Espenson, J. H.; Bakac, A. Reaction of Hydrogen Peroxide with the Oxochromium(IV) Ion by Hydride Transfer. *Inorg. Chem.* **1993**, *32*, 3162.

(32) Lubben, M.; Meetsma, A.; Wilkinson, E. C.; Feringa, B.; Que, L., Jr. Nonheme Iron Centers in Oxygen Activation: Characterization of an Iron(III) Hydroperoxide Intermediate. *Angew. Chem., Int. Ed. Engl.* **1995**, *34*, 1512.

(33) Poë, A. J.; Shaw, K.; Wendt, M. J. The *Trans*-Effect in Octahedral Complexes. III. The Kinetic and Thermodynamic *Trans*-Effects of NH<sub>3</sub> in Rhodium(III) Complexes. *Inorg. Chim. Acta* **1967**, *1*, 371.

(34) Nagao, H.; Ooyama, D.; Hirano, T.; Naoi, H.; Shimada, M.; Sasaki, S.; Nagao, N.; Mukaida, M.; Oi, T. Synthesis and Characterization of Polypyridine-ruthenium(II) Complexes Containing a Linear Ambidentate Ligand, NCO<sup>-</sup> or NCS<sup>-</sup>, and Reaction of Isocyanato Complexes under Acidic Conditions. *Inorg. Chim. Acta* **2001**, *320*, 60.

(35) A pD value in D<sub>2</sub>O was estimated based on the following equation: pD = pH + 0.4. See: Ogo, S.; Uehara, K.; Abura, T.; Watanabe, Y.; Fukuzumi, S. pH-Selective Synthesis and Structures of Alkynyl, Acyl, and Ketonyl Intermediates in Anti-Markovnikov and Markovnikov Hydrations of a Terminal Alkyne with a Water-Soluble Iridium Aqua Complex in Water. *J. Am. Chem. Soc.* **2004**, *126*, 16520.

(36) Hancock, R. D.; Martell, A. E. Ligand Design for Selective Complexation of Metal Ions in Aqueous Solution. *Chem. Rev.* **1989**, *89*, 1875.

(37) A similar disproportionation reaction was reported by Meyer et al. (ref 23a); in the reaction, a Ru(III)-NH<sub>2</sub> complex has been proposed to undergo disproportionation to afford the corresponding Ru(II)-NH<sub>3</sub> and Ru(IV)=NH complexes.

(38) Khan, M. T.; Srinivas, D.; Kureshy, R. I.; Khan, N. H. Synthesis, Characterization, and EPR Studies of Stable Ruthenium(III) Schiff Base Chloro and Carbonyl Complexes. *Inorg. Chem.* **1990**, *29*, 2320.

(39) To confirm formation of **6**, complex **2** was oxidized with an excess amount of CAN in D<sub>2</sub>O and the product was characterized with <sup>1</sup>H NMR spectroscopy (Figure S10). Consequently, distinctive signals derived from a diamagnetic Ru<sup>II</sup>-N4Py complex were

observed, and the spectrum was matched with that of the authentic [Ru<sup>II</sup>(NO<sub>2</sub>)(N4Py)] complex, which is in an acid-base equilibrium with the corresponding nitrosyl complex (ref 24). The authentic sample of [Ru(N4Py)(NO)]<sup>3+</sup> was synthesized (see the SI).

(40) Evans, D. F.; Jakubovic, D. A. Water-soluble Hexadentate Schiff-base Ligands as Sequestering Agents for Iron(III) and Gallium(III). *J. Chem. Soc., Dalton Trans.* **1988**, 2927.

(41) An <sup>1</sup>H NMR spectrum was measured for the solution of the 3e<sup>-</sup>-oxidized species of **2** formed with use of 3 equiv of [Ru<sup>III</sup>(bpy)<sub>3</sub>](ClO<sub>4</sub>)<sub>3</sub> (bpy = 2,2'-bipyridine) as an oxidant in D<sub>2</sub>O in the presence of DSS (4,4-dimethyl-4-silapentane-1-sulfonic acid) as the internal and external standards. In this study, CAN and [Ru<sup>III</sup>(bpy)<sub>3</sub>]<sup>3+</sup> were employed as oxidants. In the UV-vis and <sup>1</sup>H NMR studies, CAN was selected because it did not show absorption bands in the visible region or any <sup>1</sup>H NMR signals after the oxidation reaction. On the other hand, for the Evans method, [Ru<sup>III</sup>(bpy)<sub>3</sub>]<sup>3+</sup> was used, since [Ru<sup>II</sup>(bpy)<sub>3</sub>]<sup>2+</sup> formed after the oxidation reaction should be diamagnetic, whereas Ce<sup>III</sup> species formed from CAN after the oxidation reaction should be paramagnetic.

(42) Au, S.-M.; Huang, J.-S.; Yu, W.-Y.; Fung, W.-H.; Che, C.-M. Aziridination of Alkenes and Amidation of Alkanes by Bis-(tosylimido)ruthenium(VI) Porphyrins. A Mechanistic Study. *J. Am. Chem. Soc.* **1999**, *121*, 9120.

(43) Che, C.-M.; Yam, V. W.-W.; Mak, T. C. W. A Novel Monooxoruthenium(V) Complex Containing a Polydentate Pyridyl Amine Ligand. Syntheses, Reactivities, and X-ray Crystal Structure of [Ru<sup>III</sup>(N<sub>4</sub>O)(H<sub>2</sub>O)](ClO<sub>4</sub>)<sub>2</sub>. *J. Am. Chem. Soc.* **1990**, *112*, 2284.

(44) Luo, Y.-R. *Handbook of Bond Dissociation Energies in Organic Compounds*; CRC Press: Boca Raton, 2003.

(45) Control experiments of the three substrates oxidized by 3 equiv of CAN in the absence of complex **2** were shown in Figure S19.

(46) Zalatan, D. N.; Du Bois, J. Understanding the Differential Performance of Rh<sub>2</sub>(esp)<sub>2</sub> as a Catalyst for C-H Amination. *J. Am. Chem. Soc.* **2009**, *131*, 7558.

(47) The low reaction yield of cyclobutanone can be explained by the low reactivity of cyclobutanol, which resulted in decomposition of **5** by reaction with water molecules to afford **3** and **6** in 67% and 26% yields.

(48) Pestovsky, O.; Bakac, A. Reactivity of Aqueous Fe(IV) in Hydride and Hydrogen Atom Transfer Reactions. *J. Am. Chem. Soc.* **2004**, *126*, 13757.

(49) (a) Binstead, R. A.; Moyer, B. A.; Samuels, G. J.; Meyer, T. J. Proton-coupled Electron Transfer between [Ru(bpy)<sub>2</sub>(py)OH<sub>2</sub>]<sup>2+</sup> and [Ru(bpy)<sub>2</sub>(py)O]<sup>2+</sup>. A Solvent Isotope Effect (*k*<sub>H<sub>2</sub>O</sub>/*k*<sub>D<sub>2</sub>O</sub>) of 16.1. *J. Am. Chem. Soc.* **1981**, *103*, 2897. (b) Binstead, R. A.; Meyer, T. J. Hydrogen-atom Transfer between Metal Complex Ions in Solution. *J. Am. Chem. Soc.* **1987**, *109*, 3287.

(50) Chatterjee, S.; Sengupta, K.; Samanta, S.; Das, P. K.; Dey, A. Concerted Proton-Electron Transfer in Electrocatalytic O<sub>2</sub> Reduction by Iron Porphyrin Complexes: Axial Ligands Tuning H/D Isotope Effect. *Inorg. Chem.* **2015**, *54*, 2383.

(51) Kinetics for the oxidation reactions of 2-propanol and BnOH by **5** were also investigated in the absence of NaClO<sub>4</sub> (Figures S25 and S26); then, induction periods were observed in the early stage of the UV-vis spectral change, and the *k*<sub>C-H</sub> values were larger than those in the presence of NaClO<sub>4</sub>.

(52) Mayer, J. M. Hydrogen Atom Abstraction by Metal-Oxo Complexes: Understanding the Analogy with Organic Radical Reactions. *Acc. Chem. Res.* **1998**, *31*, 441.

(53) Tomasi, J.; Mennucci, B.; Cammi, R. Quantum Mechanical Continuum Solvation Models. *Chem. Rev.* **2005**, *105*, 2999.

(54) DFT calculations on the transition states in the oxidation of EBS by **5** were also performed to elucidate the reaction mechanism (Figure S28). Consequently, the hydride transfer mechanism was suggested to be more advantageous by 11 kcal mol<sup>-1</sup> than the hydrogen-atom transfer mechanism.